Optics Letters

Highly compact magneto-optical switches for metal-dielectric-metal plasmonic waveguides

Ali Haddadpour,[1,2] Vahid Foroughi Nezhad,[1,2] Zongfu Yu,[3] and Georgios Veronis[1,2,*]

[1]School of Electrical Engineering and Computer Science, Louisiana State University, Baton Rouge, Louisiana 70803, USA
[2]Center for Computation and Technology, Louisiana State University, Baton Rouge, Louisiana 70803, USA
[3]Department of Electrical and Computer Engineering, University of Wisconsin-Madison, Madison, Wisconsin 53706, USA
*Corresponding author: gveronis@lsu.edu

Received 20 July 2016; revised 24 August 2016; accepted 26 August 2016; posted 26 August 2016 (Doc. ID 271995); published 13 September 2016

We introduce highly compact resonant-cavity-enhanced magneto-optical switches for metal-dielectric-metal (MDM) plasmonic waveguides. The field profile of the fundamental mode of a MDM waveguide in which the metal is subject to an externally applied static magnetic field is asymmetric. The static magnetic field induced asymmetry, which enhances or reduces the coupling between the waveguide and a side-coupled resonator, and the relatively large induced wave vector modulation are used to design a Fabry–Perot cavity magneto-optical switch, consisting of a MDM waveguide side-coupled to two MDM stub resonators. The on and off states correspond to either the presence or the absence of the externally applied static magnetic field.

OCIS codes: (230.3810) Magneto-optic systems; (240.6680) Surface plasmons; (260.3910) Metal optics.

http://dx.doi.org/10.1364/OL.41.004340

Achieving active control of the flow of light in plasmonic devices is of fundamental interest in plasmonics. A possible route to actively control plasmons is to use an externally applied magnetic field [1,2]. As an example, external magnetic fields could be used to control plasmonic devices through analogies of the Kerr and Faraday effects [3,4]. Compared to electro-optics or thermo-optics, magneto-optics could lead to faster modulation speeds [2]. In addition, the magneto-optical effect breaks the time-reversal symmetry, and the use of magneto-optical materials may therefore lead to nonreciprocal plasmonic devices [5–7]. Surface plasmon polaritons propagating at metal-dielectric interfaces in which one or both media are magneto-optical have been investigated both theoretically and experimentally [8–15].

In this Letter, we introduce highly compact resonant-cavity-enhanced magneto-optical switches for metal-dielectric-metal (MDM) plasmonic waveguides. Based on the dispersion relation of the optical modes supported by a MDM waveguide in which the free-electron plasmonic metal is subject to an externally applied static magnetic field along the direction perpendicular to the plane of propagation, the field amplitude profile of the fundamental mode of the waveguide is asymmetric. The static magnetic field induced asymmetry, which can enhance or reduce the coupling between the waveguide and a side-coupled resonator, and the relatively large induced wave vector modulation can be used to design a Fabry–Perot cavity magneto-optical switch with a large modulation depth. The switch consists of a MDM waveguide side-coupled to two MDM stub resonators, and the on and off states correspond to either the presence or the absence of the externally applied static magnetic field.

A schematic of a MDM waveguide in which the metal is subject to an externally applied static magnetic field is shown in Fig. 1(a). Light in MDM waveguides can be coupled using a variety of structures such as gratings and slit-based couplers [16]. We consider TM modes, with non-zero field components E_x, E_y, and H_z. In the presence of a static magnetic field $\mathbf{B}$ in the z direction, the dielectric permittivity of the metal is described by a tensor [7,17]:

$$\bar{\bar{\varepsilon}} = 1 - \frac{\omega_P^2}{(\omega + i/\tau)^2 - \omega_B^2} \times \begin{pmatrix} 1 + i\frac{1}{\tau\omega} & i\frac{\omega_B}{\omega} & 0 \\ -i\frac{\omega_B}{\omega} & 1 + i\frac{1}{\tau\omega} & 0 \\ 0 & 0 & \frac{(\omega+i/\tau)^2-\omega_B^2}{\omega(\omega+i/\tau)} \end{pmatrix}, \quad (1)$$

where ω_P is the bulk plasmon frequency, and $\omega_B = \frac{eB}{m}$ is the cyclotron frequency. The decay time τ characterizes the material loss in the metal, e is the electron charge, and m is the electron mass. Here we use $1/\tau = 0.002\omega_P$. By applying the boundary conditions at the metal-dielectric interfaces, one can derive the following dispersion relation for the optical modes supported by the structure of Fig. 1(a) [18]:

$$\exp(2k_d w) = \frac{\left(\frac{k\varepsilon_{xy}}{\varepsilon_{xx}\varepsilon_m}\right)^2 + (k_d/\varepsilon_d - k_m/\varepsilon_m)^2}{\left(\frac{k\varepsilon_{xy}}{\varepsilon_{xx}\varepsilon_m}\right)^2 + (k_d/\varepsilon_d + k_m/\varepsilon_m)^2}, \quad (2)$$

where $\varepsilon_m = \varepsilon_{xx} + \varepsilon_{xy}^2/\varepsilon_{xx}$, k is the y component of the wave vector, $k_i = \sqrt{k^2 - k_0^2\varepsilon_i}$, $i = d, m$, and w is the width of dielectric region [Fig. 1(a)]. We observe that the above dispersion relation depends only on the square of the propagation constant k. As a result, the propagation constants for the modes propagating in the positive and negative y direction are the same.

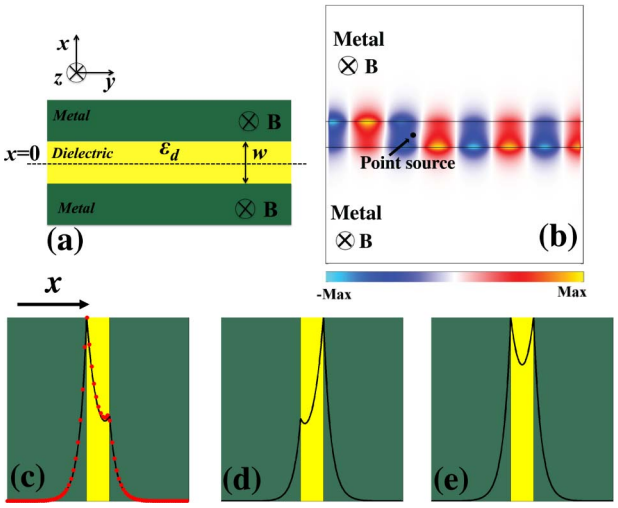

Fig. 1. (a) Schematic of a MDM waveguide. The metal is subject to an externally applied static magnetic field and has a bulk plasmon wavelength of $\lambda_P = \frac{2\pi c}{\omega_P}$, where c is the speed of light in vacuum. (b) Magnetic field distribution of propagating waves excited by a dipole source placed in the MDM waveguide structure of (a), calculated using FDFD. Results are shown for $w = 0.37\lambda_P$, $\varepsilon_d = 13.32$, $\omega = 0.16\omega_P$, $\omega_B = 0.1\omega_P$, and $1/\tau = 0.002\omega_P$. (c,d) Magnetic field amplitude profile of the fundamental TM mode propagating in the positive and negative y directions, respectively, calculated using FDFD (solid black lines), and analytically (red dots). All other parameters are as in (b). (e) Magnetic field amplitude profile of the fundamental propagating TM mode for $\omega_B = 0$. All other parameters are as in (b).

We found, however, that the corresponding field profiles are different. In Fig. 1(b) we show the magnetic field distribution of propagating waves excited by a dipole source placed in the MDM waveguide structure of Fig. 1(a) calculated with the finite-difference frequency-domain (FDFD) method [19]. We observe that, even though the right-moving and left-moving modes have the same propagation constant, the field amplitude of the right-moving (left-moving) mode is larger at the lower (upper) metal-dielectric interface.

In the absence of an externally applied static magnetic field, the magnetic field amplitude profile of the fundamental TM mode supported by the MDM waveguide has a maximum at the two metal-dielectric interfaces, and is exponentially decaying in the metal. The profile is symmetric with respect to the $x = 0$ mirror plane in the middle of the dielectric layer [Fig. 1(e)].

However, in the presence of an externally applied static magnetic field **B**, the magnetic field amplitude profile of the fundamental mode of the MDM waveguide becomes asymmetric. As in the case of no externally applied static magnetic field, the profile has a maximum at the two metal-dielectric interfaces, and the field amplitude is exponentially decaying in the metal. However, the maximum field amplitudes at the two interfaces are different, resulting in the asymmetry of the profile [13] [Figs. 1(c) and 1(d)]. In addition, because of the symmetry of the waveguide structure, the magnetic field amplitude profile of the mode propagating in the negative y direction is the mirror image with respect to the $x = 0$ plane of the profile of the mode propagating in the positive y direction [Figs. 1(c) and 1(d)]. Note that for applied magnetic field with opposite orientations below and above the dielectric there is no asymmetry in the magnetic field amplitude profile.

In Fig. 1(c), in addition to the numerically calculated magnetic field amplitude profile obtained with FDFD, we also show the analytically calculated profile, obtained by solving the dispersion relation of the modes supported by the waveguide [Eq. (2)]. We observe that there is excellent agreement between the analytical results and the numerical results obtained using the FDFD method. This demonstrates that the FDFD method that we use to model the MDM waveguide, in which the metal is subject to an externally applied static magnetic field, is indeed valid and appropriate for investigating the properties of such structures.

We now consider the effect of the externally applied static magnetic field on the propagation constant of the mode. In Fig. 2(a) we show the real part of the propagation constant in the absence ($\omega_B = 0$) and presence ($\omega_B = 0.1\omega_P$) of the static magnetic field as a function of frequency. We observe that the real part of the propagation constant of the waveguide mode in the presence of the magnetic field $\mathrm{Re}[k(\omega_B = 0.1\omega_P)]$ is larger than the real part of the propagation constant of the mode in the absence of the magnetic field $\mathrm{Re}[k(\omega_B = 0)]$. This is consistent with the dispersion relation of the modes [Eq. (2)]. To see this, for simplicity we first consider the lossless case ($1/\tau = 0$). Since for metals $\varepsilon_{xx} < 0$, we have $\varepsilon_m < 0$. In addition, the amplitude of ε_m increases when the external static magnetic field **B** is applied. As a result, the right hand side of Eq. (2) increases and, consequently, k_d; therefore, k also increases when the external static magnetic field **B** is applied. Similarly, if the effect of the loss is included ($1/\tau = 0.002\omega_P$), the real part of k increases, when the magnetic field **B** is applied [Fig. 2(a)].

We also define the magnetic field induced wave vector modulation as $|\Delta k(\omega_B)/k| \equiv |\frac{k(\omega_B)-k(\omega_B=0)}{k(\omega_B=0)}|$. We observe that, as the frequency increases, both the magnetic field induced change in the propagation constant [Fig. 2(a)], as well as

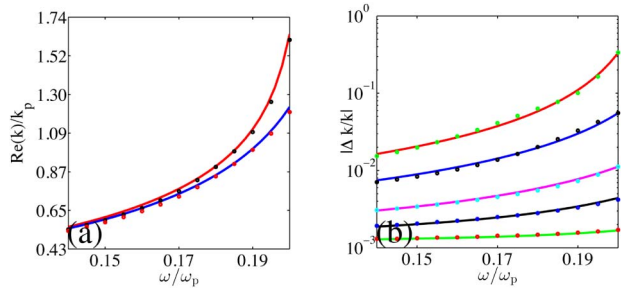

Fig. 2. (a) Real part of the y component of the wave vector, normalized by $k_P = \omega_P/c$, as a function of frequency, calculated using FDFD for $\omega_B = 0.1\omega_P$ (black dots) and $\omega_B = 0$ (red dots). Also shown are the analytically calculated results for $\omega_B = 0.1\omega_P$ (red solid line) and $\omega_B = 0$ (blue solid line). All other parameters are as in Fig. 1(b). (b) Normalized amplitude of the change in the y component of the wave vector, when the static magnetic field is applied to the metal, as a function of frequency, calculated using FDFD for $\epsilon_d = 1$ (red dots), $\epsilon_d = 3$ (blue dots), $\epsilon_d = 5$ (light blue dots), $\epsilon_d = 9$ (black dots), and $\epsilon_d = 13.32$ (green dots). Also shown are the analytically calculated results for $\epsilon_d = 1$ (solid green line), $\epsilon_d = 3$ (solid black line), $\epsilon_d = 5$ (solid pink line), $\epsilon_d = 9$ (solid blue line), and $\epsilon_d = 13.32$ (solid red line). All other parameters are as in Fig. 1(b).

the magnetic field induced wave vector modulation [Fig. 2(b)] increase. This is associated with the fact that the fraction of the modal power in the metal increases, as the frequency increases [20]. Thus, the effect of the magnetic field induced change in the dielectric permittivity of the metal on the propagation constant of the mode becomes larger, as the frequency increases.

In Fig. 2(b) we also show the effect of the dielectric permittivity ε_d of the material between the two metal regions of the MDM waveguide on the wave vector modulation $|\Delta k(\omega_B)/k|$. It is known that in a plasmonic MDM waveguide, as the permittivity of the dielectric increases, the fraction of the modal power in the metal increases [20]. Thus, we expect that the wave vector modulation $|\Delta k(\omega_B)/k|$ will increase, as the dielectric permittivity of the material between the two metal regions ε_d increases. This is indeed verified by the results shown in Fig. 2(b). The relatively large magnetic field induced wave vector modulation obtained for large ε_d can be beneficial in designing Fabry–Perot cavity magneto-optical switches [21], as we will see below.

As before, in Figs. 2(a) and 2(b), in addition to the numerically calculated results obtained with FDFD for the propagation constant of the mode and the magnetic field induced wave vector modulation, we also show the analytically calculated results, obtained by solving the dispersion relation of the modes supported by the waveguide [Eq. (2)]. Once again, we observe that there is excellent agreement between the analytical results and the numerical results obtained using the FDFD method in the whole range of parameters considered. This further demonstrates that the FDFD method that we use is appropriate for investigating the properties of such structures.

As a first step towards designing a Fabry–Perot cavity magneto-optical switch based on the structure of Fig. 1(a), we investigate a MDM waveguide side-coupled to a MDM stub resonator, when the metal is subject to an externally applied static magnetic field [Fig. 3(a)]. In Fig. 3(b), we show the transmission as a function of the stub length L_1 for the structure of Fig. 3(a). We excite the fundamental mode of the input waveguide using a point current source, and measure the power of the transmitted optical mode in the output waveguide [Fig. 3(a)]. We perform a similar simulation in a straight waveguide and the ratio of the power measured in the structure with respect to the power measured in the straight waveguide is the transmission of the structure. In the absence of an externally applied static magnetic field ($\omega_B = 0$), the transmission exhibits a dip when L_1 is equal to one of the resonant lengths of the cavity [21]. The transmission at this length is relatively low, since the incoming wave interferes destructively with the decaying amplitude into the forward direction of the resonant cavity field [22]. In the presence of an externally applied static magnetic field **B**, the transmission for the structure of Fig. 3(a) depends on the direction of the static magnetic field. When the static magnetic field is in the positive z direction ($\omega_B = 0.1\omega_P$), the magnetic field amplitude of the fundamental mode of the MDM waveguide is larger at the lower metal-dielectric interface [Fig. 1(c)]. Thus, the coupling between the waveguide and the stub resonator, which is side-coupled at the upper metal-dielectric interface, is weaker compared to the case of no externally applied static magnetic field. As a result, the on-resonance dip in transmission is smaller [Fig. 3(b)]. We also observe a shift in the resonant lengths, associated with the change in the propagation constant of the mode in the presence

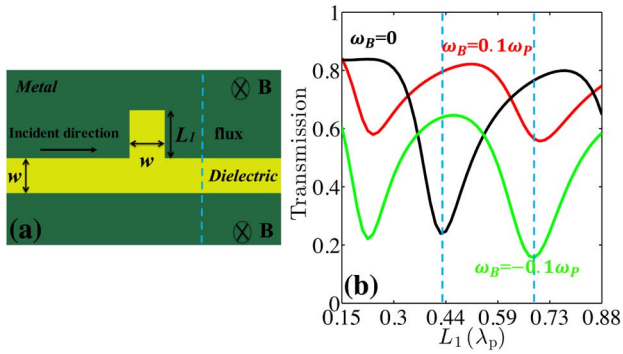

Fig. 3. (a) Schematic of a MDM waveguide side-coupled to a MDM stub resonator. The metal is subject to an externally applied static magnetic field. The dashed line indicates the flux measurement plane. (b) Transmission as a function of the stub length L_1 for the structure of (a). Results are shown for $\omega_B = 0$ (black line), $\omega_B = 0.1\omega_P$ (red line), and $\omega_B = -0.1\omega_P$ (green line). All other parameters are as in Fig. 1(b). The vertical dashed lines correspond to $L_1 = 0.43\lambda_P$ and $L_1 = 0.67\lambda_P$.

of the static magnetic field (Fig. 2). In contrast, when the static magnetic field is in the negative z direction ($\omega_B = -0.1\omega_P$), the magnetic field amplitude of the fundamental mode of the MDM waveguide is larger at the upper metal-dielectric interface [Fig. 1(d)]. Thus, the coupling between the waveguide and the stub resonator is stronger. As a result, the transmission is lower compared to the case of no externally applied static magnetic field both off-resonance and on-resonance [Fig. 3(b)].

For a MDM waveguide side-coupled to a single stub with a length of $L_1 = 0.43\lambda_P$, there is a significant difference between the transmission in the absence of an externally applied static magnetic field ($\omega_B = 0$) and the transmission when the static magnetic field is in the positive z direction ($\omega_B = 0.1\omega_P$) [Fig. 3(b)]. This significant difference in transmission can be used to design a Fabry–Perot cavity magneto-optical switch consisting of a MDM waveguide side-coupled to two MDM stub resonators, in which the metal is subject to an externally applied static magnetic field [Fig. 4(a)]. By using two stubs and properly tuning the length of the cavity L formed between them, the difference in transmission between the on and off states [Fig. 4(b)], and therefore the modulation depth of the switch, defined as $[T(\omega_B = 0.1\omega_P) - T(\omega_B = 0)]/T(\omega_B = 0.1\omega_P)$ [Fig. 4(c)], can be resonantly enhanced compared to the single-stub structure. Thus, such a Fabry–Perot cavity structure can act as a magneto-optical switch, in which the on and off states correspond to the presence/absence of an externally applied static magnetic field.

Similarly, for a waveguide side-coupled to a single stub with a length of $L_1 = 0.67\lambda_P$, there is a significant difference between the transmission in the absence of an externally applied static magnetic field ($\omega_B = 0$) and the transmission when the static magnetic field is in the negative z direction ($\omega_B = -0.1\omega_P$) [Fig. 3(b)]. Again, this difference in transmission can be used to design a Fabry–Perot cavity magneto-optical switch consisting of a MDM waveguide side-coupled to two MDM stub resonators [Fig. 4(a)], in which the on and off states correspond to the absence/presence of an externally applied static magnetic field [Figs. 4(d) and 4(e)]. Since the transmission for the single stub structure for $\omega_B = -0.1\omega_P$,

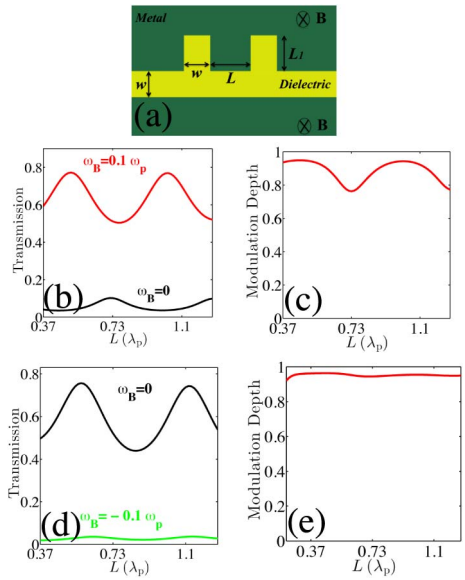

Fig. 4. (a) Schematic of a Fabry–Perot cavity structure consisting of a MDM waveguide side-coupled to two MDM stub resonators. The metal is subject to an externally applied static magnetic field. (b) Transmission as a function of the distance L between the two stubs for the structure of (a) calculated using FDFD for $\omega_B = 0$ (black line) and $\omega_B = 0.1\omega_P$ (red line). Results are shown for $L_1 = 0.43\lambda_P$. All other parameters are as in Fig. 1(b). (c) Modulation depth $[T(\omega_B = 0.1\omega_P) - T(\omega_B = 0)]/T(\omega_B = 0.1\omega_P)$ as a function of L for the structure of (a). All parameters are as in (b). (d) Transmission as a function of L for the structure of (a) calculated using FDFD for $\omega_B = 0$ (black line) and $\omega_B = -0.1\omega_P$ (green line). Results are shown for $L_1 = 0.67\lambda_P$. All other parameters are as in Fig. 1(b). (e) Modulation depth $[T(\omega_B = 0) - T(\omega_B = -0.1\omega_P)]/T(\omega_B = 0)$ as a function of L for the structure of (a). All parameters are as in (d).

$L_1 = 0.67\lambda_P$ is smaller than the one for $\omega_B = 0$, $L_1 = 0.43\lambda_P$ [Fig. 3(b)], the transmission in the off state is smaller for the double stub structure corresponding to Figs. 4(d) and 4(e), compared to the one corresponding to Figs. 4(b) and 4(c). As a result, the modulation depth as a function of the length of the cavity L is more uniform for the structure corresponding to Figs. 4(d) and 4(e).

As final remarks, a free-electron plasmonic material with the required properties is indium antimonide (InSb). For such a material, the bulk plasmon frequency is $\omega_P \simeq 12.57 \times 10^{12}$ rad/sec ($\lambda_P \simeq 150$ μm) [23] and, thus, $\omega_B = 0.1\omega_P$ corresponds to an externally applied static magnetic field of $B = 0.1$ T. The corresponding dimensions of the structure are $(w, L, L_1) \simeq (55.5, 166.5, 100.5)$ μm. In addition, the loss parameter used in this Letter ($1/\tau = 0.002\omega_P$) is appropriate for InSb [23,24]. We also found that even for a significantly larger loss parameter of $1/\tau = 0.01\omega_P$ the modulation depth is ~0.54 which is acceptable for switching applications [25]. In addition, for the structure corresponding to Figs. 4(d) and 4(e), the transmission for $\omega_B = -0.1\omega_P$ is close to zero for light incident from the left, while it is non-zero for light incident from the right. Thus, this structure could also be used for magneto-optical isolation [26]. Finally, since only the fundamental mode is propagating in each waveguide section, we can use a single-mode scattering matrix theory to account for the behavior of these systems [27]. We found that there is excellent agreement between the results obtained using such a scattering matrix theory and the exact results obtained using FDFD.

Funding. National Science Foundation (NSF) (1102301, 1254934).

REFERENCES

1. V. V. Temnov, G. Armelles, U. Woggon, D. Guzatov, A. Cebollada, A. Garcia-Martin, J.-M. Garcia-Martin, T. Thomay, A. Leitenstorfer, and R. Bratschitsch, Nat. Photonics **4**, 107 (2010).
2. S. Fan, Nat. Photonics **4**, 76 (2010).
3. M. Freiser, IEEE Trans. Magn. **4**, 152 (1968).
4. G. Armelles, A. Cebollada, A. García-Martín, and M. U. González, Adv. Opt. Mater. **1**, 10 (2013).
5. H. Zhu and C. Jiang, Opt. Lett. **36**, 1308 (2011).
6. J. B. Khurgin, Appl. Phys. Lett. **89**, 251115 (2006).
7. Z. Yu, G. Veronis, Z. Wang, and S. Fan, Phys. Rev. Lett. **100**, 023902 (2008).
8. M. S. Kushwaha and P. Halevi, Phys. Rev. B **36**, 5960 (1987).
9. K. Chiu and J. Quinn, Il Nuovo Cimento B (1971-1996) **10**, 1 (1972).
10. V. A. Dmitriev and A. O. Silva, Prog. Electromagn. Res. **21**, 177 (2011).
11. G. Armelles, A. Cebollada, A. García-Martín, J. M. García-Martín, M. U. González, J. B. González-Díaz, E. Ferreiro-Vila, and J. Torrado, J. Opt. A **11**, 114023 (2009).
12. P. Haefner, E. Luck, and E. Mohler, Phys. Status Solidi B **185**, 289 (1994).
13. D. Nikolova and A. Fisher, Phys. Rev. B **88**, 125136 (2013).
14. B. Hu, Y. Zhang, and Q. J. Wang, Nanophotonics **4**, 383 (2015).
15. E. Ferreiro-Vila, J. M. García-Martín, A. Cebollada, G. Armelles, and M. U. González, Opt. Express **21**, 4917 (2013).
16. Y. Huang, C. Min, and G. Veronis, Opt. Express **20**, 22233 (2012).
17. J. D. Jackson, *Classical Electrodynamics* (Wiley, 1998).
18. A. Haddadpour, V. Foroughi Nezhad, Z. Yu, and G. Veronis, Proc. SPIE **9546**, 95461S (2015).
19. G. Veronis and S. Fan, *Surface Plasmon Nanophotonics*, M. L. Brongersma and P. G. Kik, eds. (Springer, 2007), Vol. **131**, p. 169.
20. G. Veronis and S. Fan, J. Lightwave Technol. **25**, 2511 (2007).
21. C. Min and G. Veronis, Opt. Express **17**, 10757 (2009).
22. Y. Huang, C. Min, L. Yang, and G. Veronis, Int. J. Opt. **2012**, 372048 (2012).
23. L. Shen, X. Zheng, and X. Deng, Opt. Express **23**, 11790 (2015).
24. T. H. Isaac, W. L. Barnes, and E. Hendry, Appl. Phys. Lett. **93**, 241115 (2008).
25. W. Cai, J. S. White, and M. L. Brongersma, Nano Lett. **9**, 4403 (2009).
26. D. Jalas, A. Petrov, M. Eich, W. Freude, S. Fan, Z. Yu, R. Baets, M. Popovic, A. Melloni, J. D. Joannopoulos, M. Vanwolleghem, C. R. Doerr, and H. Renner, Nat. Photonics **7**, 579 (2013).
27. S. E. Kocabas, G. Veronis, D. A. B. Miller, and S. Fan, IEEE J. Sel. Top. Quantum Electron. **14**, 1462 (2008).